Stable Lead Succinate-Iodides with Strong Second-Harmonic Generation Response and Large Birefringence

Yulu Wu[a,b,e], Jialin Zeng[a], Ruibiao Fu[*a,d,e], Wenjing Yang[a,b,e], Zilong Geng[a,d,e], Senfu Lei[a,e], Yiting Luo[a,b,e], Xiaofan Tong[a,d,e], Zuju Ma[*c]

[a]State Key Laboratory of Structural Chemistry, Fujian Institute of Research on the Structure of Matter, Chinese Academy of Sciences, Fuzhou, Fujian 350002, P. R. China

[b]College of Chemistry and Materials Science, Fujian Normal University, Fuzhou, Fujian 350007, P. R. China

[c]School of Environmental and Materials Engineering, Yantai University, Yantai, 264005, P. R. China

[d]University of Chinese Academy of Sciences, Beijing 100049, China.

[e]Fujian College, University of Chinese Academy of Sciences, Fuzhou, Fujian 350002, P. R. China.

[*]Corresponding author. *E-mail addresses:* furb@fjirsm.ac.cn (R. B. Fu), zjma@outlook.com (Z. J. Ma).

Experimental Section

Single-Crystal X-ray Diffraction.

Single-crystal X-ray diffraction data of $(A_2I)[PbI(OOC(CH_2)_2COO)]$ (A = Rb, K) were collected on a Rigaku Saturn 724 CCD diffractometer equipped with a graphite-monochromated Mo Kα radiation. The data reduction was integrated with the program Crystal Clear version 1.30. Their structures were solved by a direct method with the aid of the SHELXT and refined by the SHELXL full-matrix least-squares program.[1, 2] Their structures were further checked by the PLATON and no higher symmetries were suggested.[3] Details of crystallographic data are listed in Tables S1-2. Atomic coordinates, equivalent isotropic displacement parameters and bond valence sum (BVS), anisotropic displacement parameters, as well as bond lengths and angles are summarized in Tables S3-S8, respectively. CCDC 2474360 for for $(Rb_2I)[PbI(OOC(CH_2)_2COO)]$ and 2474361 for $(K_2I)[PbI(OOC(CH_2)_2COO)]$.

Powder X-ray diffraction (PXRD)

PXRD measurements for $(A_2I)[PbI(OOC(CH_2)_2COO)]$ (A = Rb, K) were conducted using a Rigaku Miniflex 600 diffractometer, employing Cu Kα radiation (λ = 1.540598 Å) at room temperature. PXRD data were collected within the 2θ range of 5-55° with a step width of 0.02°.

Energy dispersive X-ray spectroscope and elemental analyses

Elemental analyses were performed by using a field emission scanning electron microscope (FESEM, JSM6700F) with an energy dispersive X-ray spectroscope (EDS, Oxford INCA). C and H analyses were carried out with a Vario EL III element analyzer.

Thermogravimetric and differential thermal analysis (TGA-DTA)

TGA-DTA of $(A_2I)[PbI(OOC(CH_2)_2COO)]$ (A = Rb, K) were employed on a NETZCH STA 449F3 thermal analysis instrument with an Al_2O_3 crucible as a reference. In a flowing nitrogen gas, the temperature was raised from 25 to 800 ^oC at a heating rate of 10 $^oC \cdot min^{-1}$.

Optical properties

According to attenuated total reflectance (ATR) method, IR spectra were as recorded on a VERTEX70 FT-IR spectrometer instrument at room temperature. The crystal sample was tightly fitted to the total reflection crystal and then the data were collected spanning over 400 to 4000 cm^{-1}.

In addition, within the wavelength range of 200-2500 nm, their UV-Vis-NIR diffuse reflectance spectra were measured using a PrkinElmer Lambda 950 ultraviolet/visible/near-infrared spectrophotometer with solid sample referenced against $BaSO_4$. The reflection spectrum was converted to absorption spectrum by using the Kubelka-Munk function: $\alpha/S = F(R) = (1–R)^2/2R$, (where S is the scattering coefficient, α is the absorption coefficient, and R is the reflectance) [4, 5].

Second-harmonic generation (SHG) measurements

Powder SHG measurements were performed on a pulsed Q-switched Nd: YAG solid-state laser with the modified Kurtz-Perry method under a wavelength of 1064 nm and room temperature.[6] Crystalline samples and microcrystalline KDP as the references were ground and sieved into progressively increasing particle size ranges: 25-45, 45-53, 53-75, 75-109, 109-150, 150-212 and 212-355 μm.

The heat-treatment procedure

Select clean and impurity-free crystals and place them on a watch glass. Then put them into an oven for the heat-treatment in the air. Then, crystals have been heated successively at 100, 150, 200 and 250°C for 30 minutes at respective temperature.

Computational details

Theoretical calculations based on density functional theory (DFT) have been performed using the Vienna *ab* initio simulation package (VASP) [7, 8] with the Perdew-Burke-Ernzerhof (PBE) [9] exchange correlation functional. The projected augmented wave (PAW) [10] potentials have been used to treat the ion-electron interactions. A Γ-centered 3×7×3 Monkhorst-Pack grid for the Clillouin zone sampling [11] and a cutoff energy of 500 eV for the plane wave expansion were found to get convergent lattice parameters and self-consistent energies. In calculation of the static $\chi^{(2)}$ coefficients, the so-called length-gauge

formalism derived by Aversa and Sipe [12] and modified by Rashkeevet al [13] is adopted, which has been proved to be successful in calculating the second order susceptibility for semiconductors and insulators.[14-16] The dynamic SHG coefficient is calculated by the formula developed by Aversa, Sipe and Rashkeev et al. [12, 13] In the static case, the imaginary part of the static second-order optical susceptibility can be expressed as:

$$\chi^{abc} = \frac{e^3}{\hbar^2\Omega}\sum_{nml,k}\frac{r^{a}_{nm}\left(r^{b}_{ml}r^{c}_{ln} + r^{c}_{ml}r^{b}_{ln}\right)}{2\omega_{nm}\omega_{ml}\omega_{ln}}[\omega_n f_{ml} + \omega_m f_{ln} + \omega_l f_{nm}]$$
$$+\frac{ie^3}{4\hbar^2\Omega}\sum_{nm,k}\frac{f_{nm}}{\omega^2_{mn}}[r^{a}_{nm}(r^{b}_{mn;c} + r^{c}_{mn;b}) + r^{b}_{nm}(r^{a}_{mn;c} + r^{c}_{mn;a}) + r^{c}_{nm}(r^{a}_{mn;b} + r^{b}_{mn;a})]$$

where r is the position operator, $\hbar\omega_{nm} = \hbar\omega_n - \hbar\omega_m$ is the energy difference for the bands m and n, $f_{mn} = f_m - f_n$ is the difference of the Fermi distribution functions, subscripts a, b, and c are Cartesian indices, and $r^{b}_{mn;a}$ is the so-called generalized derivative of the coordinate operator in k space.

$$r^{b}_{nm;a} = \frac{r^{a}_{nm}\Delta^{b}_{mn} + r^{b}_{nm}\Delta^{a}_{mn}}{\omega_{nm}} + \frac{i}{\omega_{nm}} \times \sum_{l}(\omega_{lm}r^{a}_{nl}r^{b}_{lm} - \omega_{nl}r^{b}_{nl}r^{a}_{lm})$$

where $\Delta^{a}_{nm} = (p^{a}_{nn} - p^{a}_{mm}) / m$ is the difference between the electronic velocities at the bands n and m.

The $\chi^{(2)}$ coefficients here were calculated from PBE wavefunctions with a 3×7×3 k-point grid and about 450 bands. A scissor operator has been added to correct the conduction band energy (corrected to the experimental gap), which has been proved to be reliable in predicting the second-order susceptibility for semiconductors and insulators. [17-19].

For an external radiation electric field E, the dipole moment μ_i of a group can be expressed as a Taylor series expansion [15 16]

$$\mu_i = \mu_i^0 + \alpha_{ij}E_j + \frac{1}{2!}\beta_{ijk}E_jE_k + \frac{1}{3!}\gamma_{ijkl}E_jE_kE_l$$

where i, j, k, and l subscripts represent the different Cartesian coordinate components x, y, or z. μ_i^0 is the permanent dipole moment of a group, namely the dipole moment without an applied electric field. Physical quantities α, β, and γ correspond to the linear polarizability (α, which corresponds to the linear optical coefficient of a group), first-order hyperpolarizability tensor (β, which is the second-order nonlinear optical coefficient of a group), and second-order hyperpolarizability tensor (γ, which is the third-order nonlinear optical coefficient of a group).

We calculate the static linear polarizability (α) and static first-order hyperpolarizability (β) of [PbI_2O_4] and [$OOC(CH_2)_2COO$] groups at the PBE1PBE level [9] of theory with a reasonably large basis set def2TZVP [20, 21] by using the Gaussian 09 program.[22] The polarizability anisotropy ($\Delta\alpha$) was obtained by the following formula to reflect the sources of birefringence.[23]

$$\Delta\alpha = \sqrt{\left[\left(\alpha_{xx} - \alpha_{yy}\right)^2 + \left(\alpha_{xx} - \alpha_{zz}\right)^2 + \left(\alpha_{yy} - \alpha_{zz}\right)^2\right]/2}$$

Table S1. Crystal data and structural refinements for (Rb_2I)[$PbI(OOC(CH_2)_2COO)$].

Empirical formula	(Rb_2I)[$PbI(OOC(CH_2)_2COO)$]
Formula weight	748.00

Temperature(K)	293(2)
Crystal color	Colorless
Wavelength(Å)	0.71073
Crystal system	Orthorthombic
Space group	*Ima*2
a / Å	12.0622(11)
b / Å	6.8832(5)
c / Å	15.0775(15)
α / °	90
β / °	90
γ / °	90
Volume / Å^3	1251.83(19)
Z	4
Absorption correction	spherical harmonics
Crystal size	0.3 mm × 0.3 mm × 0.3 mm
ρ_{calcd} / g·cm^{-3}	3.969
μ / mm^{-1}	26.118
F(000)	1288.0
Data / restraints / parameters	2573/1/66
2-Theta range for data collection	5.404 to 68.82
Limiting indices	-19 ≤h ≤ 19,-10≤K≤10, -21≤1≤23
Reflections collected / unique	9899
Independent reflections	2573 [R_{int}=0.0399, R_{sigma}=0.0284]
Completeness	100%
Goodness-of-fit on F^2	1.086
R_1,wR_2 (I > 2σ) [a]	R_1 = 0.0353, wR_2 = 0.0824
R_1,wR_2 (all data)	R_1 = 0.0409, wR_2 = 0.0846
Largest diff. peak and hole/ e·Å^{-3}	1.39 / -1.52
Flack parameter	-0.017(6)

[a]$R_1 = \Sigma||F_o| - |F_c||/\Sigma|F_o|$ and $wR_2 = [\Sigma w(Fo^2 - Fc^2)^2/ \Sigma wF_o^4]^{1/2}$.

Table S2. Crystal data and structural refinements for $(K_2I)[PbI(OOC(CH_2)_2COO)]$.

Empirical formula	$(K_2I)[PbI(OOC(CH_2)_2COO)]$
Formula weight	655.26
Temperature(K)	297.77(10)

Crystal color	Colorless
Wavelength(Å)	0.71073
Crystal system	Orthorthombic
Space group	*Ima*2
a / Å	11.7525(5)
b / Å	6.8495(3)
c / Å	15.1124(7)
α / °	90
β / °	90
γ / °	90
Volume / Å^3	1216.53(9)
Z	4
Absorption correction	spherical harmonics
Crystal size	0.3 mm × 0.3 mm × 0.3 mm
ρ_{calcd} / g·cm^{-3}	3.578
μ / mm^{-1}	19.609
F(000)	1144
Data / restraints / parameters	1659/1/65
2-Theta range for data collection	5.392 to 60.832
Limiting indices	$-15 \le h \le 14$, $-8 \le k \le 9$, $-20 \le l \le 21$
Reflections collected	6944
Independent reflections	1659 [Rint=0.0420, R_{sigma}=0.0379]
Completeness	100%
Goodness-of-fit on F^2	1.068
R_1,wR_2 ($I > 2\sigma$) [a]	R_1 = 0.0264, wR_2 = 0.0564
R_1,wR_2 (all data)	R_1 = 0.0329, wR_2 = 0.0585
Largest diff. peak and hole/ e·Å^{-3}	0.65 / -1.18
Flack parameter	0.004(5)

[a] $R_1 = \Sigma||F_o| - |F_c||/\Sigma|F_o|$ and $wR_2 = [\Sigma w(Fo^2 - Fc^2)^2/ \Sigma wF_o^4]^{1/2}$.

Table S3. Atomic coordinates, equivalent isotropic displacement parameters (Å^2) and BVS for (Rb_2I)[$PbI(OOC(CH_2)_2COO)$].

Atom	***Wyck.***	***x***	***y***	***z***	U_{eq}[a]	**BVS**[b]
Pb1	4a	0.5	0.5	0.43766(2)	0.02573(13)	1.69

I1	4a	0.25	0.52394(14)	0.34849(9)	0.0333(2)	-0.72
I2	4b	0	1	0.33644(7)	0.03 (2)	
Rb1	4b	0.75	0.4609(2)	0.66416(13)	0.0378(4)	0.78
Rb2	4b	0.25	1.01317(14)	0.47054(13)	0.0308(3)	1.10
O1	8c	0.5979(5)	0.6887(8)	0.5519(5)	0.0351(13)	-2.07
O2	8c	0.4178(5)	0.7549(8)	0.5556(4)	0.0322(12)	-1.87
C1	8c	0.5156(6)	0.7779(11)	0.5849(6)	0.0267(16)	
C2	8c	0.5362(10)	0.9097(13)	0.6614(6)	0.039(2)	

[a]U_{eq} is defined as 1/3 of the trace of the orthogonalisedU_{ij} tensor.

[b]Bond valence sums were calculated by the equation：$s = \exp[(R_0 - R_i)/b]$, where R_0 and b are the bond valence parameters and R_i is the observed bond lengths.

Table S4. Atomic coordinates, equivalent isotropic displacement parameters (Å^2) and BVS for $(K_2I)[PbI(OOC(CH_2)_2COO)]$.

Atom	***Wyck.***	***x***	***Y***	***z***	U_{eq}[a]	**BVS[b]**
Pb1	4a	0.5	0.5	0.56589(2)	0.0319(14)	1.71
I1	4a	1	0	0.66338(7)	0.0397(3)	
I2	4b	0.75	0.53391(14)	0.65554(9)	0.048(3)	-0.70
K1	4b	0.75	0.5383(4)	0.3501(3)	0.0499(8)	0.72
K2	4b	0.75	0.0125(3)	0.5295(3)	0.0441(8)	0.91
O1	8c	0.5997(5)	0.3076(8)	0.4506(4)	0.0428(14)	-2.00
O2	8c	0.4148(5)	0.2465(8)	0.4456(4)	0.0394(14)	-1.90
C1	8c	0.5139(6)	0.2221(12)	0.4161(6)	0.032(19)	
C2	8c	0.5363(10)	0.915(13)	0.3404(6)	0.044(2)	

[a]U_{eq} is defined as 1/3 of the trace of the orthogonalisedU_{ij} tensor.

[b]Bond valence sums were calculated by the equation：$s = \exp[(R_0 - R_i)/b]$, where R_0 and b are the bond valence parameters and R_i is the observed bond lengths.

Table S5. Anisotropic displacement parameters (Å^2) for $(Rb_2I)[PbI(OOC(CH_2)_2COO)]$.

Atom	U_{11}	U_{22}	U_{33}	U_{23}	U_{13}	U_{12}
Pb1	0.02058(18)	0.0327(2)	0.0239(2)	0	0	-0.0025(12)
I1	0.0195(4)	0.0455(10)	0.0351(5)	-0.0005 (4)	0	0
I2	0.0309(9)	0.0313(4)	0.0279(5)	0	0	0.0005(2)
Rb1	0.0294(6)	0.0463(8)	0.0376(8)	0.0068(6)	0	0
Rb2	0.0291(5)	0.0334(5)	0.035(7)	-0.0039(4)	0	0
O1	0.033(3)	0.031(3)	0.041(4)	0(3)	-0.004(3)	0.002(2)
O2	0.034(3)	0.031(3)	0.032(3)	-0.005(2)	-0.002(3)	0(2)
C1	0.034(4)	0.021(3)	0.025(4)	0.006(3)	-0.004(3)	-0.003(2)
C2	0.075(6)	0.025(4)	0.016(4)	0.001(3)	-0.017(4)	-0.004(4)

Table S6. Anisotropic displacement parameters (Å^2) for $(K_2I)[PbI(OOC(CH_2)_2COO)]$.

Atom	U_{11}	U_{22}	U_{33}	U_{23}	U_{13}	U_{12}
Pb1	0.024(2)	0.0396(2)	0.0321(3)	0	0	0.00247(14)

I1	0.049(7)	0.0321(5)	0.0379(6)	0	0	-0.0004(2)
I2	0.0216(4)	0.0758(6)	0.0465(6)	0.0107(7)	0	0
K1	0.0362(15)	0.0471(17)	0.066(3)	0.0074(15)	0	0
K2	0.0327(16)	0.0478(16)	0.052(2)	0.0068(11)	0	0
O1	0.038(3)	0.041(3)	0.049(4)	0.003(3)	0.004(3)	-0.002(2)
O2	0.033(3)	0.044(3)	0.041(4)	-0.005(3)	0.003(3)	0.003(2)
C1	0.042(5)	0.024(3)	0.030(4)	0.006(3)	0.004(4)	0.004(3)
C2	0.076(6)	0.031(4)	0.026(5)	0.002(3)	0.017(4)	0.004(5)

Table S7. Selected bond lengths (**Å)** and angles (deg.) for $(Rb_2I)[PbI(OOC(CH_2)_2COO)]$.

Pb(1)-O(1)	2.459(6)	Pb(1)-O(2)$^{\#1}$	2.687(6)
Pb(1)-O(1)$^{\#1}$	2.459(6)	Pb(1)-I(1)	3.3058(6)
Pb(1)-O(2)	2.687(6)	Pb(1)-I(1)$^{\#1}$	3.3058(6)
O(1)-Pb(1)-O(1)$^{\#1}$	91.1(3)	O(1)$^{\#1}$-Pb(1)-I(1)$^{\#1}$	134.15(14)
O(1)-Pb(1)-O(2)	50.9(2)	O(2)-Pb(1)-O(2)$^{\#1}$	97.2(3)
O(1)-Pb(1)-O(2)$^{\#1}$	72.8(2)	O(2)-Pb(1)-I(1)	84.26(13)
O(1)-Pb(1)-I(1)	134.15(14)	O(2)-Pb(1)-I(1)$^{\#1}$	129.65(13)
O(1)-Pb(1)-I(1)$^{\#1}$	82.72(15)	O(2)$^{\#1}$-Pb(1)-I(1)	129.65(13)
O(1)$^{\#1}$-Pb(1)-O(2)	72.8(2)	O(2)$^{\#1}$-Pb(1)-I(1)$^{\#1}$	84.26(13)
O(1)$^{\#1}$-Pb(1)-O(2)$^{\#1}$	50.9(2)	I(1)-Pb(1)-I(1)$^{\#1}$	132.01(4)
O(1)$^{\#1}$-Pb(1)-I(1)	82.72(15)		

Symmetry transformations used to generate equivalent atoms: #1 1 - x, 1 - y, z.

Table S8. Selected bond lengths (**Å)** and angles (deg.) for $(K_2I)[PbI(OOC(CH_2)_2COO)]$.

Pb(1)-O(1)	2.479(6)	Pb(1)-O(2)$^{\#1}$	2.706(6)
Pb(1)-O(1)$^{\#1}$	2.479(6)	Pb(1)-I(2)	3.2437(6)
Pb(1)-O(2)	2.707(6)	Pb(1)-I(2)$^{\#1}$	3.2438(6)
O(1)-Pb(1)-O(1)$^{\#1}$	90.7(3)	O(1)$^{\#1}$-Pb(1)-I(2)$^{\#1}$	84.47(14)
O(1)-Pb(1)-O(2)	50.3(2)	O(2)-Pb(1)-O(2)$^{\#1}$	95.6(3)
O(1)-Pb(1)-O(2)$^{\#1}$	72.19(19)	O(2)-Pb(1)-I(2)	131.43(12)
O(1)-Pb(1)-I(2)	84.47(14)	O(2)-Pb(1)-I(2)$^{\#1}$	84.23(12)
O(1)-Pb(1)-I(2)$^{\#1}$	84.47(14)	O(2)$^{\#1}$-Pb(1)-I(2)	84.23(12)
O(1)$^{\#1}$-Pb(1)-O(2)	72.20(19)	O(2)$^{\#1}$-Pb(1)-I(2)$^{\#1}$	131.43(12)
O(1)$^{\#1}$-Pb(1)-O(2)$^{\#1}$	50.3(2)	I(2)-Pb(1)-I(2)$^{\#1}$	130.63(5)
O(1)$^{\#1}$-Pb(1)-I(2)	133.12(13)		

Symmetry transformations used to generate equivalent atoms: #1 1 - x, 1 - y, z.

Table S9. The local dipole moment (μ) in Debye, as well as polarizability anisotropy ($\Delta\alpha$) for four $[PbI_2O_4]$ polyhedrons and four $[OOC(CH_2)_2COO]$ groups in per unit cell of $[Rb_2I][PbI(OOC(CH_2)_2COO)]$. The charge of the structural group was estimated by the Bader charge of each atom.

Dipole moment	μ_x	μ_y	μ_z	μ	$\Delta\alpha$
$[PbI_2O_4]$	0.00	0.00	-18.14	18.14	37.89
$[PbI_2O_4]$	0.00	0.00	-18.14	18.14	37.89
$[PbI_2O_4]$	0.00	0.00	-18.14	18.14	37.89
$[PbI_2O_4]$	0.00	0.00	-18.14	18.14	37.89
$[OOC(CH_2)_2COO]$	0.00	0.00	4.81	4.81	29.65
$[OOC(CH_2)_2COO]$	0.00	0.00	4.81	4.81	29.65
$[OOC(CH_2)_2COO]$	0.00	0.00	4.81	4.81	29.65
$[OOC(CH_2)_2COO]$	0.00	0.00	4.81	4.81	29.65
Total	0.00	0.00	-53.32		

Table S10. The first-order hyperpolarizability (β) in 10^{-30} esu for four $[PbI_2O_4]$ polyhedrons and four $[OOC(CH_2)_2COO]$ groups in per unit cell of $(Rb_2I)[PbI(OOC(CH_2)_2COO)]$.

First-order hyperpolarizability	***x***	***y***	***z***
$[PbI_2O_4]$	0.00	0.00	420.67
$[PbI_2O_4]$	0.00	0.00	420.67
$[PbI_2O_4]$	0.00	0.00	420.67
$[PbI_2O_4]$	0.00	0.00	420.67
$[OOC(CH_2)_2COO]$	0.00	0.00	1.83
$[OOC(CH_2)_2COO]]$	0.00	0.00	1.83
$[OOC(CH_2)_2COO]$	0.00	0.00	1.83
$[OOC(CH_2)_2COO]$	0.00	0.00	1.83

Table S11. The local dipole moment (μ) in Debye, as well as polarizability anisotropy ($\Delta\alpha$) for four $[PbI_2O_4]$ polyhedrons and four $[OOC(CH_2)_2COO]$ groups in per unit cell of $(K_2I)[PbI(OOC(CH_2)_2COO)]$. The charge of the structural group was estimated by the Bader charge of each atom.

Dipole moment	μ_x	μ_y	μ_z	μ	$\Delta\alpha$
$[PbI_2O_4]$	0.00	0.00	18.8	18.8	17.2
$[PbI_2O_4]$	0.00	0.00	18.8	18.8	17.2
$[PbI_2O_4]$	0.00	0.00	18.8	18.8	17.2
$[PbI_2O_4]$	0.00	0.00	18.8	18.8	17.2
$[OOC(CH_2)_2COO]$	0.00	0.00	-4.84	4.84	29.32
$[OOC(CH_2)_2COO]$	0.00	0.00	-4.84	4.84	29.32
$[OOC(CH_2)_2COO]$	0.00	0.00	-4.84	4.84	29.32
$[OOC(CH_2)_2COO]$	0.00	0.00	-4.84	4.84	29.32
Total	0.00	0.00	55.84		

Table S12. The first-order hyperpolarizability (β) in 10^{-30} esu for four $[PbI_2O_4]$ polyhedrons and four $[OOC(CH_2)_2COO]$ groups in per unit cell of $(K_2I)[PbI(OOC(CH_2)_2COO)]$.

First-order hyperpolarizability	***x***	***y***	***z***
$[PbI_2O_4]$	0.03	-0.05	-174.61
$[PbI_2O_4]$	-0.05	0.08	-174.59
$[PbI_2O_4]$	0.01	0.01	-174.64
$[PbI_2O_4]$	0.03	-0.04	-174.62
$[OOC(CH_2)_2COO]$	0.00	0.00	-2.39
$[OOC(CH_2)_2COO]$	0.00	0.00	-2.39
$[OOC(CH_2)_2COO]$	0.00	0.00	-2.39
$[OOC(CH_2)_2COO]$	0.00	0.00	-2.39

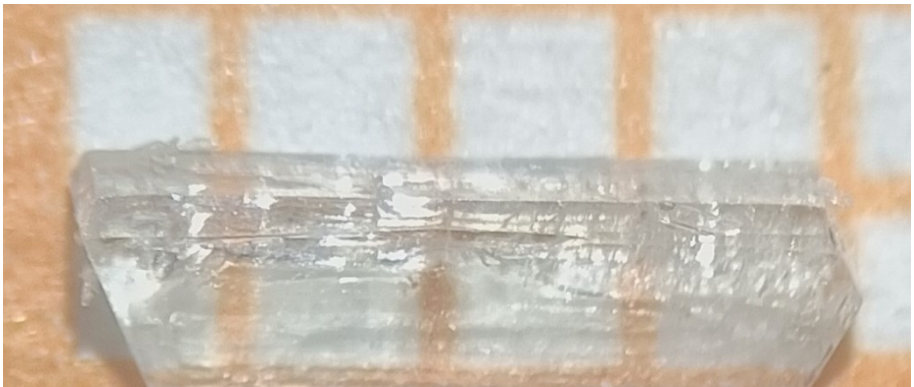

Figure S1. A photograph of the as-grown crystal without polishing for (Rb_2I)[PbI($OOCCH_2CH_2COO$)].

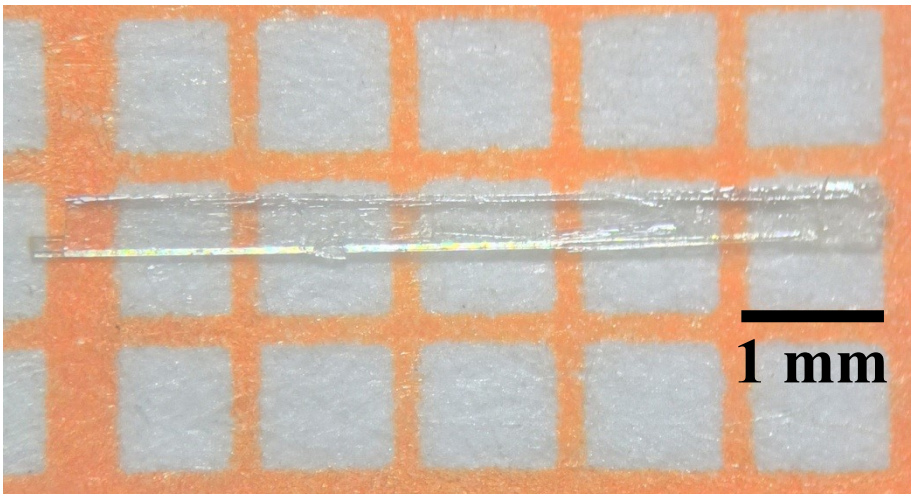

Figure S2. A photograph of the as-grown crystal without polishing for (K_2I)[PbI($OOCCH_2CH_2COO$)].

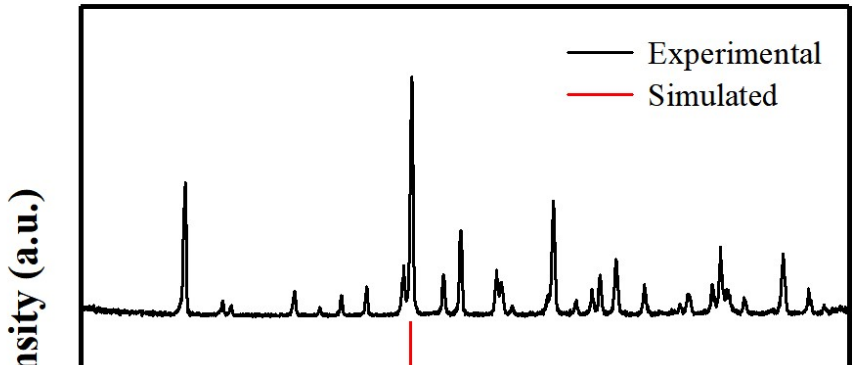

Figure S3. Experimental and simulated PXRD patterns of $(Rb_2I)[PbI(OOC(CH_2)_2COO)]$.

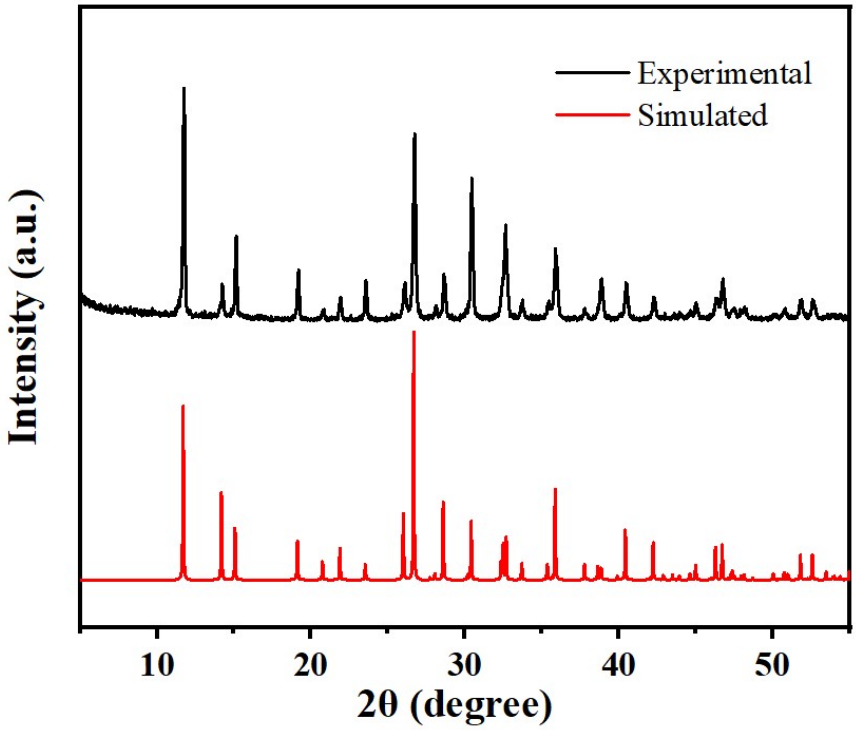

Figure S4. Experimental and simulated PXRD patterns of $(K_2I)[PbI(OOC(CH_2)_2COO)]$.

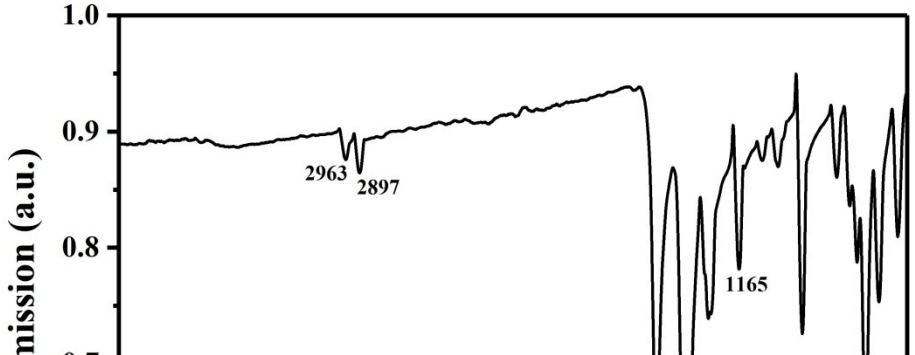

Figure S5. The IR spectrum of $(Rb_2I)[PbI(OOC(CH_2)_2COO)]$.

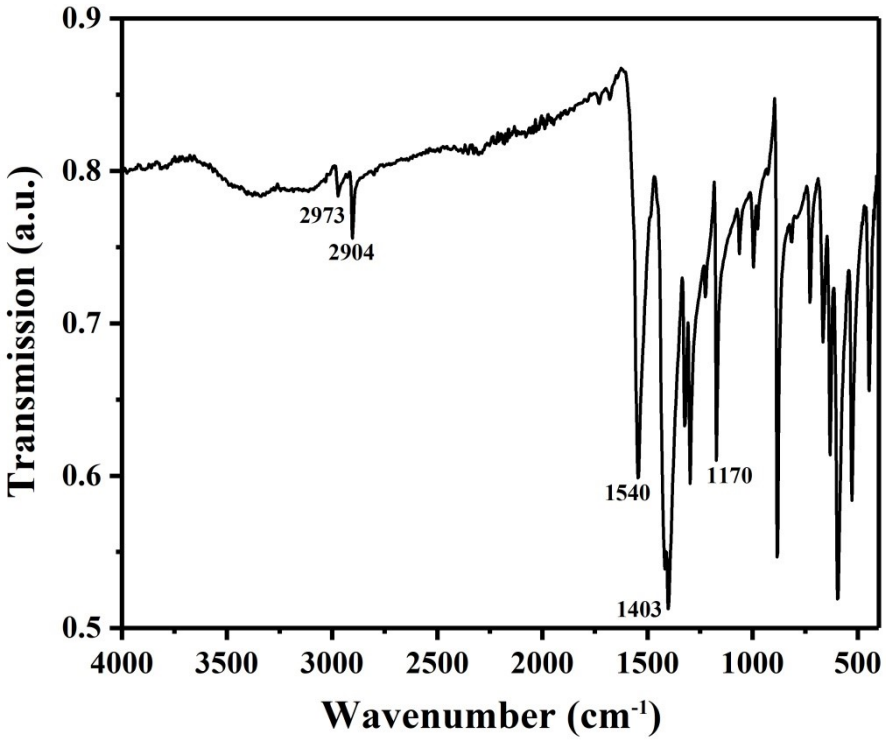

Figure S6. The IR spectrum of $(K_2I)[PbI(OOC(CH_2)_2COO)]$.

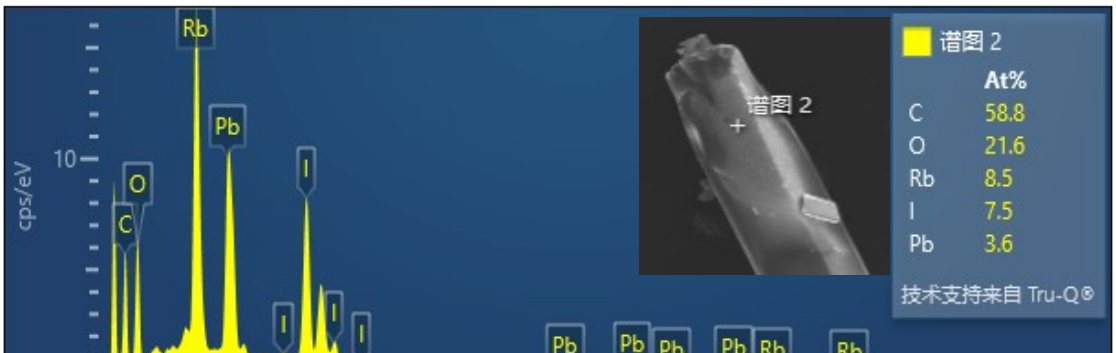

Figure S7. The EDS spectrum of $(Rb_2I)[PbI(OOC(CH_2)_2COO)]$.

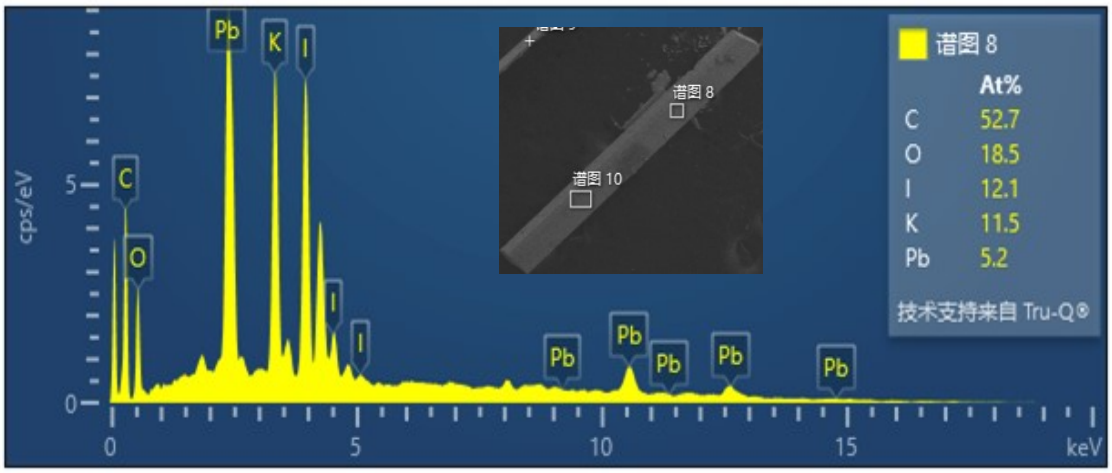

Figure S8. The EDS spectrum of $(K_2I)[PbI(OOC(CH_2)_2COO)]$.

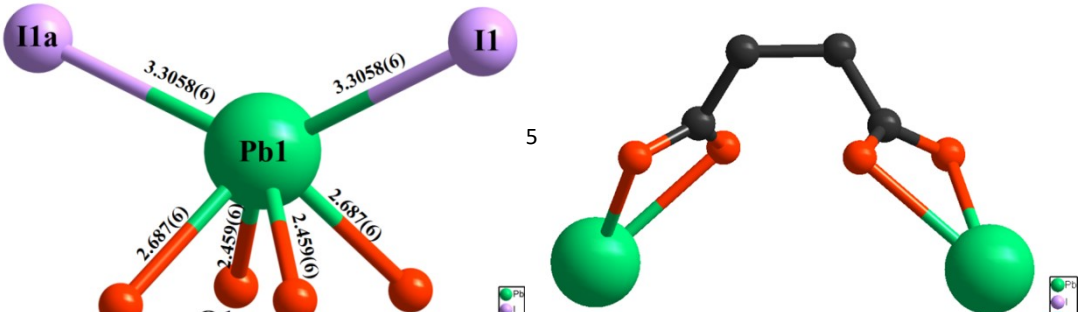

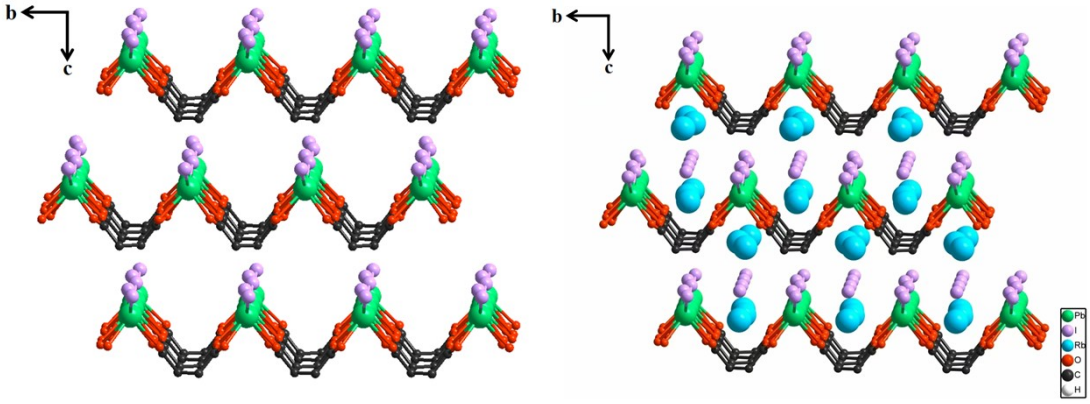

(e) **(f)**

Figure S9. (a) The coordination environment of the Pb(II) atom in $(Rb_2I)[PbI(OOC(CH_2)_2COO)]$. (b) The coordination mode of the succinate group. The environments of (c) the $Rb1^+$ and (d) the $Rb2^+$ cations. (e) The uniform alignment of the wave-like layers. (f) The structure of $(Rb_2I)[PbI(OOC(CH_2)_2COO)]$. Symmetry codes: a 1 - x, 1 - y, z; b 1- x, - 0.5 + y, 0.5 + z; c 1.5 - x, y, z; d 0.5 + x, 1 - y, z; e 0.5 + x, - 0.5 + y, 0.5 + z; f - 0.5 + x, 2 - y, z; g 1 - x, 2 - y, z; h 0.5 - x , y, z; i x, 1 + y, z.

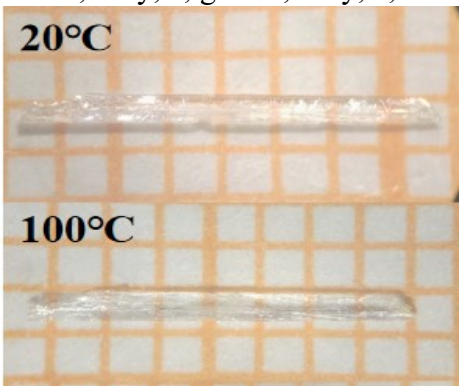

Figure S10. Photographs were taken of $(K_2I)[PbI(OOC(CH_2)_2COO)]$ crystals after heat-treatment at 100, 150, 200 and 250 °C for 30 minutes in air, respectively.

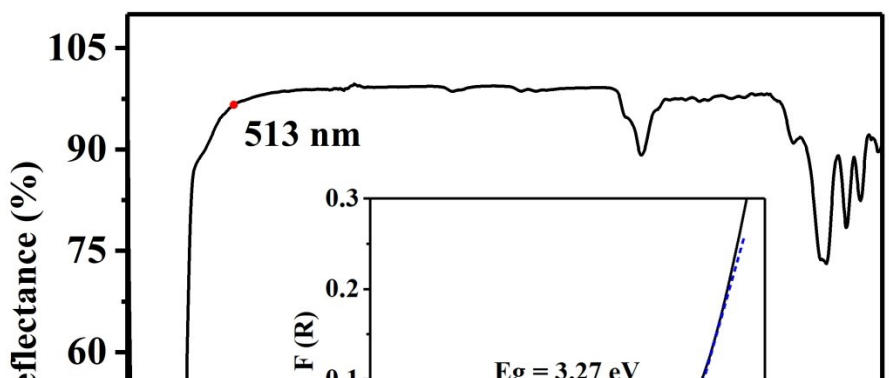

Figure S11. The UV-Vis-NIR spectrum of $(Rb_2I)[PbI(OOC(CH_2)_2COO)]$. Inset: the bandgap of $(Rb_2I)[PbI(OOC(CH_2)_2COO)]$.

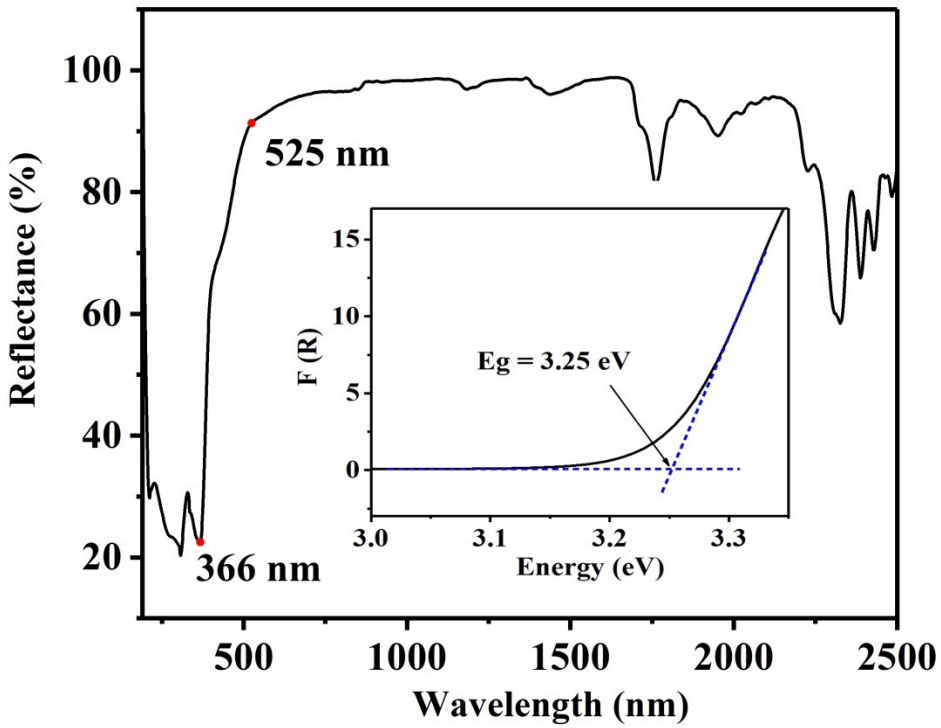

Figure. S12. The UV-Vis–NIR spectrum of $(K_2I)[PbI(OOC(CH_2)_2COO)]$. Inset: the bandgap of $(K_2I)[PbI(OOC(CH_2)_2COO)]$.

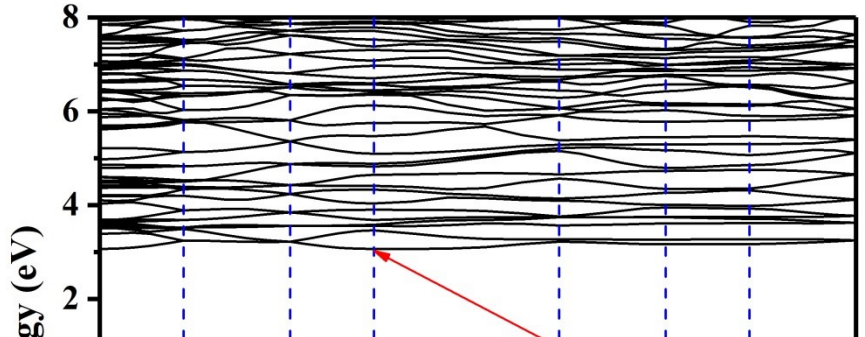

Figure S13. The calculated band structure of (Rb_2I)[PbI(OOC(CH_2)$_2$COO)].

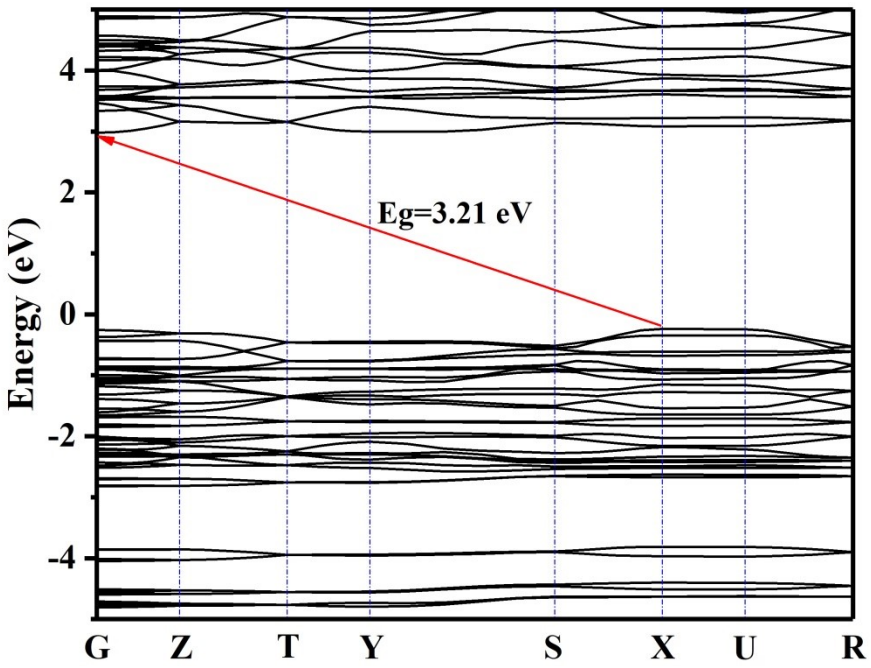

Figure S14. The calculated band structure of (K_2I)[PbI(OOC(CH_2)$_2$COO)].

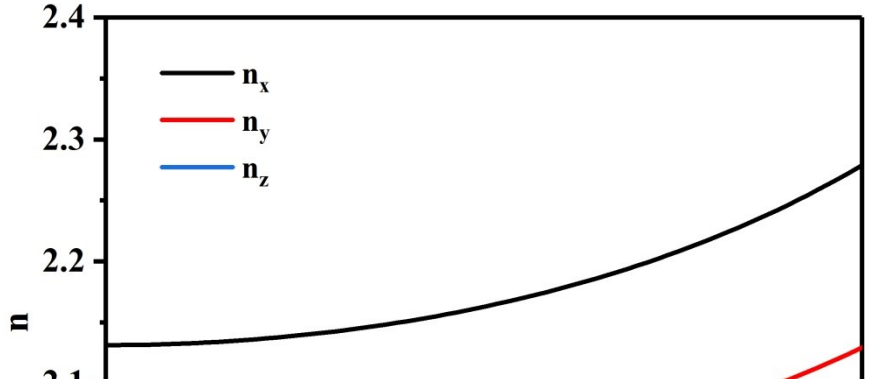

Figure S15. Optical refractive indices along principal axes *versus* photon energy for $(Rb_2I)[PbI(OOC(CH_2)_2COO)]$.

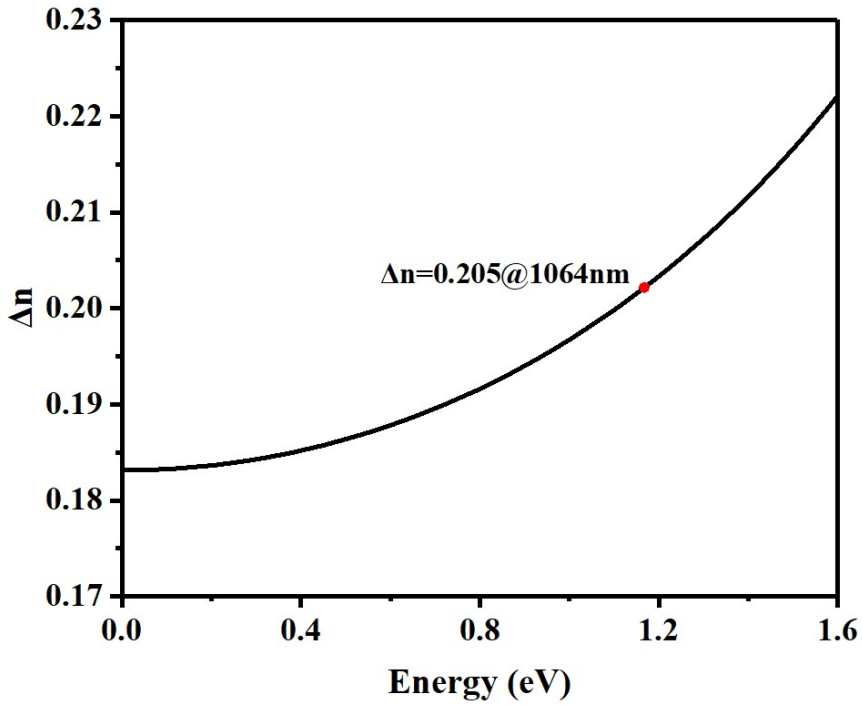

Figure S16. The calculated birefringence *versus* photon energy for $(Rb_2I)[PbI(OOC(CH_2)_2COO)]$.

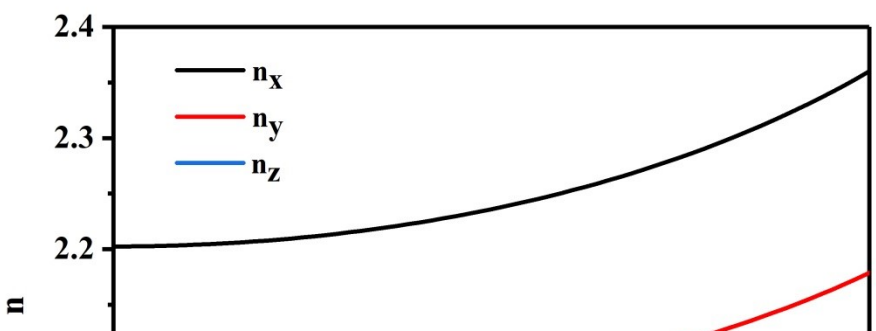

Figure S17. Optical refractive indices along principal axes *versus* photon energy for $(K_2I)[PbI(OOC(CH_2)_2COO)]$.

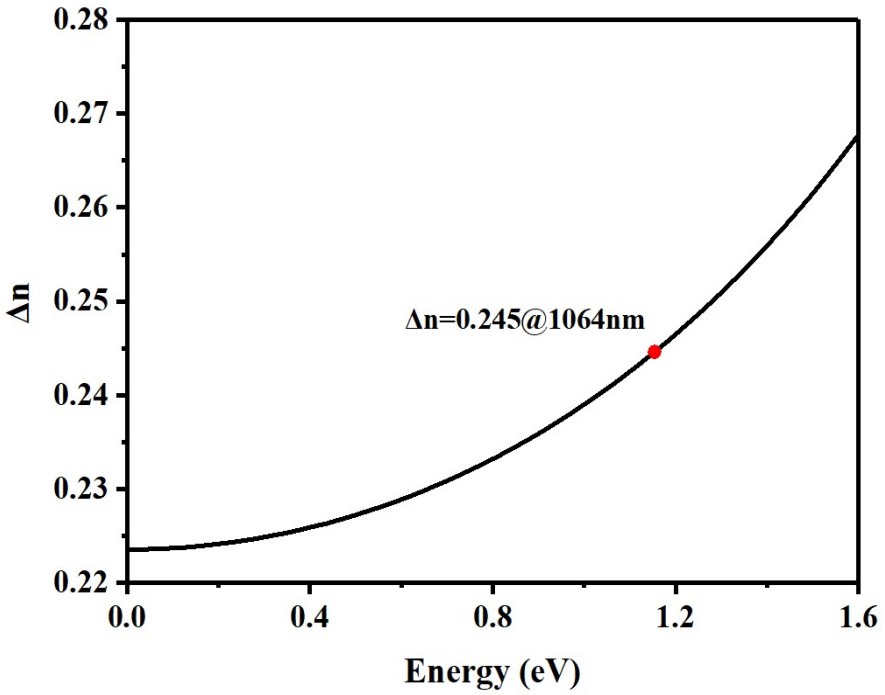

Figure S18. The calculated birefringence *versus* photon energy for $(K_2I)[PbI(OOC(CH_2)_2COO)]$.

References

[1] G. M. Sheldrick, Crystal structure refinement with SHELXL, *Acta Crystallogr. C Struct. Chem.* 2015, **71**, 3-8.

[2] G. M. Sheldrick, SHELXT-integrated space-group and crystal-structure determination, *Acta Crystallogr. A.* 2015, **71**, 3-8.

[3] A. L. Spek, Single-crystal structure validation with the program PLATON, *J. Appl. Crystallogr.* 2003, **36**, 7-13.

[4] P. Kubelka, F. Munk, An article on optics of paint layers, *Z. Tech. Phys.* 1931, **12**, 259-274.

[5] J. Tauc, Absorption edge and internal electric fields in amorphous semiconductors, Mater. Res. Bull. 1970, **5**, 721-729.

[6] S. Kurtz, T. Perry, A powder technique for the evaluation of nonlinear optical materials, *J. Appl. Phys.* 1968, **39**, 3798-3813.

[7] G. Kresse, J. Furthmüller, Efficient iterative schemes for *ab* initio total-energy calculations using a plane-wave basis set, *Phys. Rev. B. Condens. Matter.* 1996, **54**, 11169-11186.

[8] G. Kresse, D. Joubert, From ultrasoft pseudopotentials to the projector augmented-wave method, *Phys. Rev. B.* 1999, **59**, 1758-1775.

[9] J. P. Perdew, K. Burke, M. Ernzerhof, Generalized gradient approximation made simple, *Phys. Rev. Lett.* 1996, **77**, 3865-3868.

[10] P. E. Blochl, Projector augmented-wave method, *Phys. Rev. B Condens. Matter.* 1994, **50**, 17953-17979.

[11] H. J. Monkhorst, J. D. Pack, Special points for brillouin-zone integrations, *Phys. Rev. B.* 1976, **13**, 5188-5192.

[12] C. Aversa, J. Sipe, Nonlinear optical susceptibilities of semiconductors: results with a length-gauge analysis, *Phys. Rev. B.* 1995, **52**, 14636-14645.

[13] S. N. Rashkeev, W. R. L. Lambrecht, B. Segall, Efficient *ab* initio method for the calculation of frequency-dependent second-order optical response in semiconductors, *Phys. Rev. B.* 1998, **57**, 3905-3919.

[14] Z. X. Fang, J. Lin, R. Liu, P. Liu, Y. Li, X. Huang, K. N. Ding, L. X. Ning, Y. F. Zhang, Computational design of inorganic nonlinear optical crystals based on a

genetic algorithm, *Cryst. Eng. Comm.* 2014, **16**, 10569-10580.

[15] Y. C. Yang, X. Liu, J. Lu, L. M. Wu, L. Chen, $[Ag(NH_3)_2]_2SO_4$: A strategy for the coordination of cationic moieties to design nonlinear optical materials, *Angew. Chem. Int. Ed.* 2021, **60**, 21216-21220..

[16] Z. Ma, J. Hu, R. Sa, Q. Li, Y. Zhang, K. Wu, Screening novel candidates for mid-IR nonlinear optical materials from I_3-V-VI_4 compounds, *J. Mater. Chem. C.* 5 2017, **5**, 1963-1972.

[17] Y. Z. Huang, L. M. Wu, X. T. Wu, L. H. Li, L. Chen, Y. F. Zhang, $Pb_2B_5O_9I$: an iodide borate with strong second harmonic generation, *J. Am. Chem. Soc.* 2010, **132**, 12788-12789.

[18] B. Champagne, D. M. Bishop, Calculations of nonlinear optical properties for the solid state, *Adv. Chem. Phys.* 2003, **126**, 41-92.

[19] A. H. Reshak, S. Auluck, I. V. Kityk, Specific features in the band structure and linear and nonlinear optical susceptibilities of $La_2CaB_{10}O_{19}$ Crystals, *Phys. Rev. B.* 75 2007, **75**, 245120.

[20] F. Weigend, R. Ahlrichs, Balanced basis sets of split valence, triple zeta valence and quadruple zeta valence quality for H to Rn: design and assessment of accuracy, *Phys. Chem. Chem. Phys.* 2005, **7**, 3297-3305.

[21] F. Weigend, Accurate coulomb-fitting basis sets for H to Rn, *Phys. Chem. Chem. Phys.* 2006, **8**, 1057-1065.

[22] M. J. Frisch, G. W. Trucks, H. B. Schlegel, G. E. Scuseria, M. A. Robb, J. R. Cheeseman, G. Scalmani, V. Barone, G. A. Petersson, H. Nakatsuji, X. Li, M. Caricato, A. Marenich, J. Bloino, B. G. Janesko, R. Gomperts, B. Mennucci, H. P. Hratchian, J. V. Ortiz, A. F. Izmaylov, J. L. Sonnenberg, D. Williams-Young, F. Ding, F. Lipparini, F. Egidi, J. Goings, B. Peng, A. Petrone, T. Henderson, D. Ranasinghe, V. G. Zakrzewski, J. Gao, N. Rega, G. Zheng, W. Liang, M. Hada, M. Ehara, K. Toyota, R. Fukuda, J. Hasegawa, M. Ishida, T. Nakajima, Y. Honda, O. Kitao, H. Nakai, T. Vreven, K. Throssell, J. A. Montgomery, Jr., J. E. Peralta, F. Ogliaro, M. Bearpark, J. J. Heyd, E. Brothers, K. N. Kudin, V. N. Staroverov, T. Keith, R. Kobayashi, J. Normand, K. Raghavachari, A. Rendell, J. C. Burant, S. S. Iyengar, J.

Tomasi, M. Cossi, J. M. Millam, M. Klene, C. Adamo, R. Cammi, J. W. Ochterski, R. L. Martin, K. Morokuma, O. Farkas, J. B. Foresman, and D. J. Fox, Gaussian 09, Revision A.02, Gaussian, Inc., Wallingford CT, 2016.

[23] T. Lu, F. Chen, Multiwfn: A multifunctional wavefunction analyzer, *J. Comput. Chem.* 2012, **33**, 580-592.